Interference-Resistant Radar Reception With Microwave Photonic Time-Frequency Matched Signal Selection and Amplification

Gengze Wu, *Graduate Student Member, IEEE*, Fangzheng Zhang, *Senior Member, IEEE*, Xiaoyue Yu, *Graduate Student Member, IEEE*, Hao Wang, *Graduate Student Member, IEEE*, Chenchang Zeng, Zhenyu Xu, Shilong Pan, *Fellow, IEEE*, and Kai Wang

***Abstract*—Traditional radar receivers are confronted with severe challenges posed by strong in-band interference. Such interference signals often drive the low-noise amplifier (LNA)-based receiver into saturation, resulting in spectral regrowth and the generation of intermodulation distortion products (IMPs). To address this critical issue, an interference-resistant radar reception method based on microwave photonic time-frequency matched signal selection and amplification (TFM-SSA) is proposed in this paper. The core foundation of this method lies in a Dynamic sideband amplification injection locking (SAIL) mechanism in an optically injected semiconductor laser (OISL) system. By properly controlling the current of the slave laser (SL), the narrowband gain spectrum (GS) generated by period-one (P1) oscillation can be designed to dynamically sweep to match the instantaneous frequency of the signal of interest (SOI). Based on the Dynamic SAIL mechanism and considering the distinct time-frequency characteristics of the SOI and in-band interference, the proposed TFM-SSA method selectively amplifies the SOI that matches the designed GS in time-frequency domain, while effectively suppressing the strong interference before the receiver enters saturation. In the experiment, the properties of Dynamic SAIL are investigated, and the reception of a 4-GHz bandwidth linear frequency-modulated (LFM) signal interfered by parallel interference and cross interference signals is demonstrated, respectively. Experimental results verify the effectiveness of the Dynamic SAIL-based TFM-SSA method in reducing the noise floor and improving the target peak-to-floor ratio (PFR). This not only eliminates the generation of false targets but also enhances the radar's detection sensitivity under high-power interference conditions. Therefore, the proposed TFM-SSA method can provide a powerful solution for addressing the in-band interference encountered by current radar receivers.**

***Index Terms*—Microwave photonics, optically-injected laser, signal selection and amplification.**

Received 3 April 2026; revised 13 May 2026; accepted 21 May 2026. Date of publication 25 May 2026; date of current version 16 July 2026. This work was supported in part by the Natural Science Foundation of China under Grant 62371224, in part by the Shanghai Aerospace Science and Technology Innovation Foundation under Grant SAST2024-023, in part by the Open Found of IPOC (BUPT), and in part by the Aviation Science Foundation of China under Grant 2015ZC52024. *(Corresponding author: Fangzheng Zhang.)*

Gengze Wu, Fangzheng Zhang, Xiaoyue Yu, Hao Wang, Chenchang Zeng, and Shilong Pan are with the National Key Laboratory of Microwave Photonics, Nanjing University of Aeronautics and Astronautics, Nanjing 210016, China (e-mail: zhangfangzheng@nuaa.edu.cn).

Zhenyu Xu is with the Shanghai Institute of Satellite Engineering, Shanghai 201111, China.

Kai Wang is with the China Electronics Technology Group Corporation No.38 Research Institute, Hefei 230094, China.

Color versions of one or more figures in this article are available at https://doi.org/10.1109/JLT.2026.3696528.

Digital Object Identifier 10.1109/JLT.2026.3696528

I. Introduction

RADAR technology is now playing a pivotal role across a diverse spectrum of applications ranging from the Internet of Things (IoT) and smart cities to autonomous systems [1], [2], [3]. Compared with other sensors, radar possesses the unique capabilities of all-weather, day-and-night, and long-range observation. However, the explosive growth in the number of radar sensors has led to a severely congested electromagnetic environment [4], [5], [6]. The conventional radar reception based on low-noise amplifier (LNA) and bandpass filter (BPF) [7] could effectively deal with out-of-band interference. When the interference shares the same frequency band as the radar operating signals, conventional frequency-domain filtering becomes ineffective in dealing with the in-band interference. In this regard, developing methods to mitigate or eliminate the impact of in-band interference presents a pressing challenge for future radar systems.

Previously, extensive research on in-band interference-resistant radar reception has primarily relied on digital signal processing (DSP). In [8], a method using wavelet denoising to extract and suppress mutual interference in the time domain was proposed. Meanwhile, considerable research based on adaptive noise cancellation (ANC) algorithm to deal with the increased noise floor due to radar interference has been reported [9], [10]. Moreover, in [11], a constant false alarm rate (CFAR) detector-based approach is proposed, which detects interference in the time-frequency domain and applies masking or amplitude correction to recover the signal. Current DSP methods rely on the premise of linear reception. However, high-power interference often saturates the LNA prior to digitization, generating severe intermodulation products (IMPs). These nonlinearities corrupt the signal features, thereby misleading the DSP algorithms and making interference suppression ineffective [12]. Consequently, it is essential to implement interference-resistant radar reception in the analog domain before the signal reaches the LNA and analog-to-digital converter (ADC). Yet, such architectures have rarely been reported.

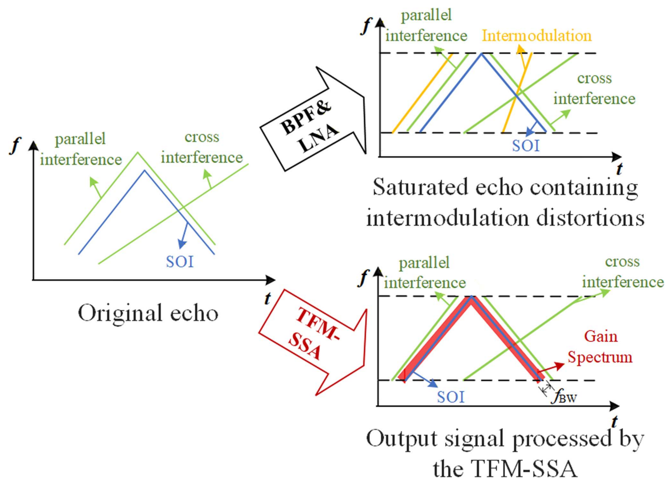

Fig. 1. Schematic of the conventional radar reception and proposed interference-resistant radar reception based on TFM-SSA method.

Microwave photonic technology [13], [14], [15] offers significant advantages in bandwidth and tunability, providing a promising path for enhancing radar interference resistance. Currently, photonic-assisted analog-domain solutions primarily focus on interference cancellation [16], [17], [18], [19], which cancels interference via precise amplitude and phase matching with a reference signal. However, these methods are limited to self-interference scenarios where a reference is available. Besides, stimulated Brillouin scattering (SBS)-based anti-interference techniques have also been explored. In [20], an SBS-based signal processor suppresses high-power interference by exploiting power-dependent energy transfer, which fundamentally relies on a sufficient power disparity between interference and signal rather than their distinct time-frequency characteristics. Consequently, its effectiveness degrades significantly when the interference power is comparable to that of the SOI. In this paper, to address the previous limitations, we exploit the distinct waveform characteristics of the signal of interest (SOI) compared to the interference in the time-frequency domain and propose a microwave photonic time-frequency matched signal selection and amplification (TFM-SSA) method to implement interference-resistant radar reception. This method can selectively amplify the SOI while suppressing mismatched interference power directly in the optical domain. Specifically, the proposed TFM-SSA method is realized by an optically injected semiconductor laser (OISL) system [21], [22], [23], utilizing its inherent sideband amplification injection locking (SAIL) effect [24], [25] for radio frequency (RF) signal amplification in the optical domain. As the conventional SAIL effect typically operates with a static gain spectrum (GS) and thus cannot process wideband radar signals, we introduce a Dynamic SAIL mechanism to tune the GS within the period-one (P1) oscillation state of an OISL system. Herein, the Dynamic SAIL is implemented by directly modulating the bias current of the slave laser (SL), so that the GS dynamically and synchronously matches the instantaneous frequency of the SOI. This mechanism serves as the core of the TFM-SSA, enabling selective amplification within the time-frequency domain while suppressing strong interferences. In this paper, we explain the principle and implementation of the TFM-SSA method based on the Dynamic SAIL mechanism, experimentally investigate its properties, and verify the performance of interference-resistant radar reception under various interference scenarios. The results validate that the proposed method can effectively eliminate false targets and significantly improve radar detection sensitivity under high-power interference.

The subsequent sections of this article are structured as follows. Section II details the principle and theoretical analysis of interference-resistant radar reception with TFM-SSA based on the Dynamic SAIL mechanism. In Section III, performance of Dynamic SAIL mechanism is characterized, and interference-resistant capability of the TFM-SSA method is experimentally demonstrated under different interference scenarios. Finally, Section IV draws conclusions.

II. Principle

This section is organized into two parts: Firstly, the principle of interference-resistant radar reception using the proposed TFM-SSA method is presented. Secondly, the implementation of the TFM-SSA method based on Dynamic SAIL mechanism is detailed, followed by a theoretical analysis of its time-frequency domain signal amplification capability.

A. Radar Reception with TFM-SSA Method

In practical scenarios, radar receivers encounter diverse interference signals with distinct time-frequency characteristics. For example, parallel interference maintains a fixed frequency offset with the same chirp rate, generating distinct false targets in range profiles; whereas cross interference intersects the SOI with a different chirp rate, severely elevating the noise floor and masking weak targets. Due to these varying characteristics, conventional DSP-based approaches often require specific algorithm modifications tailored to each interference type, limiting their universal applicability. To overcome this, we exploit the fundamental distinction that unintentional interference characteristics differ from the victim radar's transmitted waveform in the time-frequency domain. Consequently, it is feasible to selectively amplify the SOI while suppressing the interference power directly in the optical domain. This approach is referred to as the TFM-SSA method. A key advantage of this method is its universality: regardless of the specific interference type (e.g., cross or parallel interference), it can effectively achieve interference suppression. The operation principles of the conventional radar reception and the proposed TFM-SSA method are compared schematically in Fig. 1. The original echo diagram on the left illustrates the time-frequency characteristics of the echo signals, which contain the SOI (blue line) and two types of typical interferences (green lines): parallel interference and cross interference. Although these interferences share the same frequency band as the SOI, they exhibit distinct time-frequency characteristics. Specifically, the parallel interference has the same chirp rate as the SOI but maintains a fixed frequency offset, whereas the cross interference has a different chirp rate and only intersects the SOI temporarily. When processed by a conventional radar reception employing a BPF and an LNA (upper path), the strong in-band interferences drive the LNA into nonlinear saturation. As depicted in the figure, this saturation not only compresses the gain of the SOI but also generates severe IMPs (yellow lines). In contrast, the proposed TFM-SSA method (lower path) exploits the aforementioned time-frequency characteristics differences. Since the interferences only overlap with the SOI in the frequency band but do not completely overlap in the instantaneous time domain, a tunable narrowband GS (marked by the red area with a bandwidth of f_{BW}) is generated. This GS is controlled to synchronously match the instantaneous frequency of the SOI. Consequently, the SOI is effectively covered by the GS and achieves coherent amplification. Meanwhile, the strong interference signals, being mismatched in the time-frequency domain, fall outside the instantaneous window of the GS and are effectively suppressed. Such analog optical-domain signal selection fundamentally prevents the receiver front-end from entering nonlinear saturation.

It is worth noting that, in practical applications, the proposed method can be integrated into a cognitive radar framework. Initially, the radar operates in surveillance mode to perform a coarse scan of the environment and identify potential regions of interest (ROIs). Once strong interference is detected or when the radar needs to track specific targets within an ROI, the TFM-SSA method is activated. By adjusting the time delay of the control signal to match the round-trip time of the targets in the ROI, this method enables the receiver to selectively amplify the SOI from specific ranges [26], [27], effectively acting as a tunable gate in the optical domain. Furthermore, the proposed method is effective for various waveform types, including linear frequency-modulated and frequency-hopping signals.

B. TFM-SSA Realized By Dynamic SAIL Mechanism

The proposed TFM-SSA method is implemented based on an OISL system of which the structure is shown in Fig. 2(a). A continuous-wave optical carrier f_{m} generated by a tunable master laser (ML) is directed into a Mach-Zehnder modulator (MZM), which is driven by the radar received signal comprising the SOI and the interference. This modulated optical signal is then injected into the SL via an optical circulator (CIR). Under proper injection conditions, the SL operates in P1 oscillation state, creating a narrowband GS inherent to the SAIL effect [28]. As illustrated by the spectral evolution in Fig. 2(b), prior to injection, the modulated optical signal consists of f_{m} and $\pm$1st modulation sidebands ($f_{\mathrm{m}}\pm f_{\mathrm{RF}}$). Upon optical injection, the free-running SL mode f_{s} undergoes a red-shift to $f_{\mathrm{s}}^{'}$, accompanied by a surrounding narrowband GS. When the -1st sideband falls within this GS, it captures the optical gain and is selectively amplified, resulting in an asymmetric output spectrum. However, this static SAIL effect only provides a fixed amplification window, which is inadequate for processing wideband radar signals.

To address the limitation of a fixed GS, we introduce the Dynamic SAIL mechanism. The center frequency of the GS is intrinsically linked to P1 oscillation frequency, which can be flexibly tuned by adjusting the bias current of the SL. Taking advantage of this characteristic, we introduce a GS controller into the OISL system. By directly modulating the SL with a pre-designed time-varying control signal, the GS controller drives the central frequency of the GS to sweep dynamically according to the instantaneous frequency variation of the SOI. Subsequently, the selectively amplified optical signal emitted from the SL is injected to a photodetector (PD) for optical-to-electrical (O/E) conversion. The operation principle of the Dynamic SAIL is detailed in Fig. 2(c). In this derivation, both the SOI and the interference are linear frequency modulation (LFM) signals. Although they overlap in both the time and frequency domains, they exhibit distinct characteristics in the time-frequency domain. Fig. 2(c-i) depicts the optical spectrum after modulation by the MZM, in which the SOI with a starting frequency of f_{soi} and a bandwidth of B_1, and the interference with a starting frequency of f_{int} and a bandwidth of B_2 are

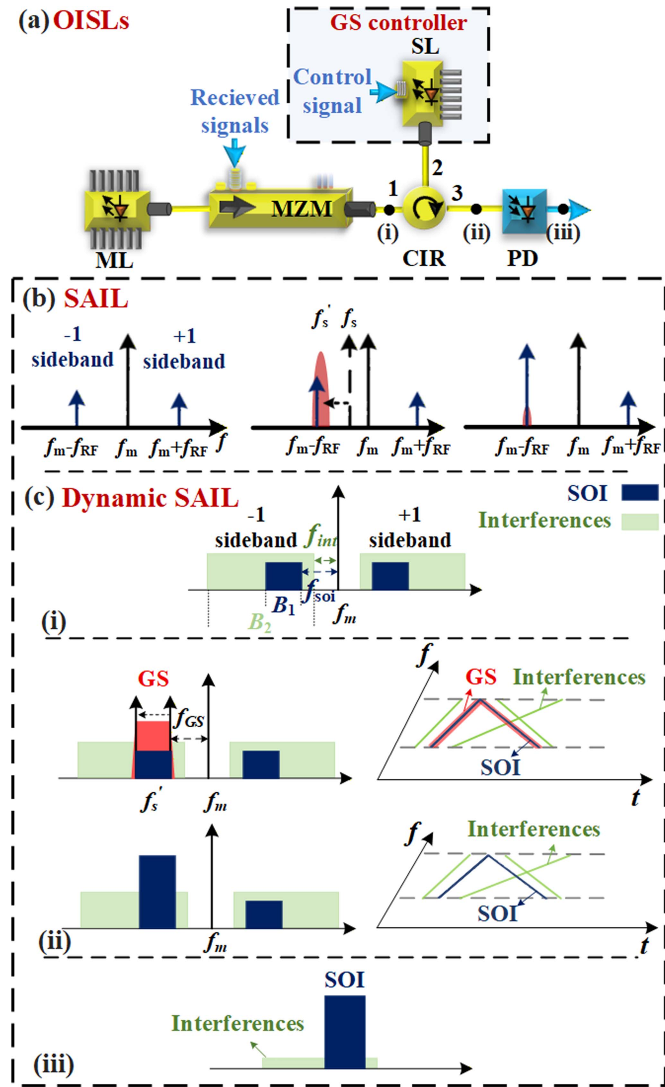

Fig. 2. (a) Schematic of the OISL system and the GS controller for Dynamic SAIL. Operating principle of the (b) static SAIL and (c) Dynamic SAIL mechanism: (i) optical spectrum of the received signals after modulation; (ii) implement of time-frequency domain matching; and (iii) the selectively amplified output signal after O/E conversion.

modulated onto the optical carrier, generating ± 1 modulation sidebands. This way, the time-frequency characteristics of both the SOI and the interference signal are mapped to the optical modulation sidebands. When the bias current of the SL is fast changed by applying a control signal, both carrier-induced and thermal-induced refractive index modulations are excited. Given the microsecond timescale of the control signal, the thermal effect, which is governed by the heat diffusion process in the active region, dominates the wavelength tuning process [29]. Consequently, the achievable chirp rate of the gain spectrum sweep is fundamentally limited by the thermal time constant of the laser active region; currently reported chirp rates of directly modulated semiconductor lasers typically range from approximately 0.01 GHz/μs [30] to 0.5 GHz/μs [31], which is nonetheless sufficient for wideband radar applications. Under this thermally dominated regime, the bias current modulation induces a periodic temperature oscillation that directly varies the effective refractive index, thereby shifting the SL's longitudinal cavity mode. As the center frequency of the GS is intrinsically linked to the cavity mode of the SL, the GS is dynamically swept back and forth across a wide spectral range in accordance with the control signal, enabling the Dynamic SAIL mechanism. The regenerated optical carrier is fixed at f_{m}, while the red-shifted cavity mode at f_{s}' is tuned over time, causing the Dynamic SAIL effect that leads to fast variation of the GS. As shown in Fig. 2(c-ii), if the amplitude and time of the control signal are properly pre-designed, the instantaneous GS sweeps in strict accordance with the time-frequency characteristics of the SOI. Specifically, the sweeping range of the GS is tuned to exactly cover the bandwidth B_1, and its temporal phase is aligned with the SOI pulse. As a result, the -1st sideband of the SOI remains temporally and spectrally aligned with the dynamic GS, thereby receiving coherent amplification. Conversely, the interference signals, possessing different chirp rates or starting frequencies, are mismatched with the GS. As shown in Fig. 2(c-iii), the mismatched interference signals fall outside the instantaneous amplification window, undergoing severe power suppression during the subsequent O/E conversion.

To rigorously analyze the time-frequency domain signal amplification capability of the TFM-SSA method based on Dynamic SAIL mechanism, we establish a mathematical model. The radar received signal S_{in}(t), consisting of SOI and interference, is a superposition of two LFM waveforms:

$$S_{in}(t) = A_1 \exp\left[j\left(2\pi f_{soi} t + \pi \frac{B_1}{T_1} t^2\right)\right] + A_2 \exp\left[j\left(2\pi f_{\mathrm{int}} t + \pi \frac{B_2}{T_2} t^2 + \phi_{\mathrm{int}}\right)\right] \quad (1)$$

where A_1, T_1, f_{soi} and A_2, T_2, f_{int} are the amplitudes, time durations and starting frequencies of SOI and interference, respectively, and φ_{int} represents the initial phase difference. The instantaneous frequency of the SOI and the interference can be derived as

$$f_{\mathrm{inst},1}(t) = f_{\mathrm{soi}} + \frac{B_1}{T_1} t \quad (2)$$

$$f_{\mathrm{inst},2}(t) = f_{\mathrm{int}} + \frac{B_2}{T_2} t \quad (3)$$

According to [32] and [33], the GS of SAIL effect behaves as a regenerative amplifier, of which the frequency response can be approximated as a Lorentzian function. For Dynamic SAIL mechanism, by modifying the standard Lorentzian model to include time and frequency dependency, the time-frequency domain power gain function $G(t, f)$ is formulated as:

$$G(t, f) = \frac{G_{\max}}{1 + \left(\frac{f_{\mathrm{inst}}(t) - f_{\mathrm{GS}}(t)}{f_{\mathrm{BW}}/2}\right)^2} \quad (4)$$

where $G_{\max}$ is the peak gain, f_{BW} is the 3-dB bandwidth of the GS and $f_{\mathrm{inst}}(t)$ denotes the instantaneous frequency of the input signal component under evaluation (corresponding to either $f_{\mathrm{inst},1}$ or $f_{\mathrm{inst},2}$).

To realize signal selection and amplification, the control signal drives $f_{\mathrm{GS}}(t)$ to match the instantaneous frequency of the SOI. Under this condition, the frequency detuning between the SOI and the GS remains zero throughout the duration ($f_{\mathrm{inst},1}(t)$-$f_{\mathrm{GS}}(t) \approx 0$). By substituting the instantaneous frequencies into (4), we derive the effective gain

$$G_{\mathrm{soi}}(t) \approx G_{\max} \quad (5)$$

This indicates that the SOI is coherently amplified by the peak gain constantly. In contrast, for the interference signal, its instantaneous frequency differs from that of SOI in time-frequency domain. The effective gain of interference $G_{\mathrm{int}}(t)$ becomes

$$G_{\mathrm{int}}(t) = \frac{G_{\max}}{R_{\mathrm{rej}}(t)} \quad (6)$$

where $R_{\mathrm{rej}}(t)$ represents high rejection ratio derived from the denominator of the Lorentzian function

$$R_{\mathrm{rej}}(t) = 1 + \left(\frac{f_{\mathrm{inst},2}(t) - f_{\mathrm{GS}}(t)}{f_{\mathrm{BW}}/2}\right)^2 = 1 + \left(\frac{2}{f_{\mathrm{BW}}} \cdot \left[(f_{\mathrm{int}} - f_{\mathrm{soi}}) + \left(\frac{B_2}{T_2} - \frac{B_1}{T_1}\right) t\right]\right)^2 \quad (7)$$

Equation (6) quantitatively demonstrates the suppression mechanism: as the time t evolves, the rejection ratio $R_{\mathrm{rej}}(t)$ increases quadratically due to bandwidth mismatch. This results in a rapid decay of the interference gain away from the intersection point. Consequently, the total output power P_{out} can be approximated as:

$$P_{\mathrm{out}}(t, f) \approx G_{\max} \cdot |A_1|^2 + \frac{G_{\max}}{R_{rej}(t)} \cdot |A_2|^2 \quad (8)$$

In (8), the first term represents the amplification of the SOI with $G_{\max}$, and the second term explicitly demonstrates the interference suppression mechanism, where the effective gain applied to the interference is significantly attenuated by $R_{\mathrm{rej}}(t)$. As theoretically indicated by (7), a narrower f_{BW} yields a higher $R_{\mathrm{rej}}(t)$, thereby providing enhanced suppression of signals with mismatched time-frequency characteristics. This theoretical derivation verifies that TFM-SSA method effectively realizes simultaneous SOI amplification and interference suppression.

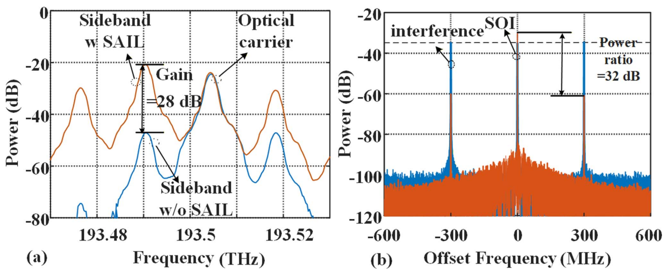

Fig. 3. The (a) optical spectrum and (b) corresponding electrical spectrum, plotted against the offset frequency relative to 15 GHz, of the unprocessed signals (blue lines) and processed signals (orange lines).

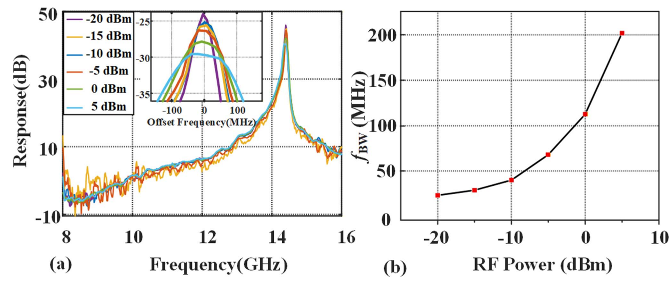

Fig. 4. The (a) frequency response of the GS with different output RF powers of VNA and the zoom-in view, (b) The measured 3-dB f_{BW} as a function of the RF power.

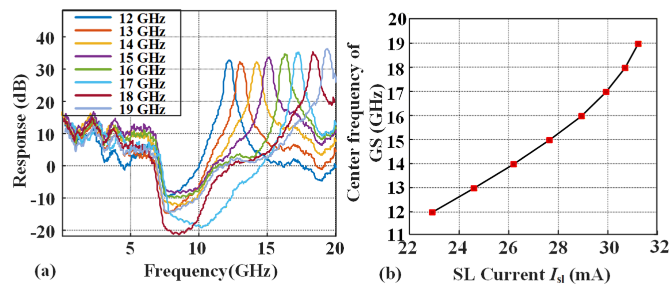

Fig. 5. (a) The frequency response of GS under different SL bias currents I_{sl} (b) the relation between center frequency of GS and I_{sl}.

III. Experiments and Results

This section presents the experimental research in two parts. Firstly, the properties of the Dynamic SAIL mechanism are investigated, and secondly, the interference-resistant radar reception based on the TFM-SSA method is experimentally validated.

A. *Properties of Dynamic SAIL Mechanism*

For a better understanding of the Dynamic SAIL mechanism, the capability of static SAIL effect in selecting and amplifying a single-tone signal while suppressing unintentional interference is analyzed. In the experiment, the frequency and output power of the ML are set to 193.502 THz and 16 dBm, respectively. The bias current and temperature of the SL are set to 26.8 mA and 26 °C. The unprocessed signals, including the single-tone SOI with frequency of 15 GHz and interference signals with frequency of 14.7 and 15.3 GHz, are generated by an arbitrary waveform generator (AWG). These signals, with a power of 0 dBm, are modulated onto the optical carrier via an MZM biased at the quadrature point. The optical spectrum and corresponding electrical spectrum of the unprocessed signals (blue lines) and processed signals (orange lines) after SAIL are shown in Fig. 3. As shown in Fig. 3(a), the sideband is amplified by 28 dB, compared with the sideband without SAIL effect. Fig. 3(b) illustrates the electrical domain results. Without SAIL effect, the power levels of SOI and interference are comparable. However, when the GS spectrally overlaps with the SOI, the latter is amplified while the interference power is suppressed, yielding a power difference of 32 dB between the two signals.

Then, the influence of input RF signal power on the f_{BW} is characterized. The frequency response is measured via a vector network analyzer (VNA, R&S ZVA67), in which the VNA output drove the MZM biased at quadrature point while the output signal from the PD is fed back to the input port of the VNA. The frequency response lines acquired under different RF output power levels are presented in Fig. 4(a). As indicated in the zoom-in view, the spectral width of the GS broadens as the RF power increases. This trend is quantitatively summarized in Fig. 4(b). As the RF output power is increased from -20 dBm to 5 dBm, the f_{BW} expands from approximately 40 MHz to 200 MHz. It is important to note that the GS bandwidth does not decrease indefinitely and it converges to a lower bound determined by the intrinsic linewidth of the SL, typically in the range of tens of MHz at low RF powers [32]. For relatively high injection power of 5 dBm, the maximum achievable static bandwidth is limited to around 200 MHz. Such a bandwidth constraint is insufficient for processing wideband radar signals.

To address this limitation, the frequency tunability of the instantaneous GS center frequency is exploited. Accordingly, the tunability of the GS center frequency via changing the SL bias current (I_{sl}) is experimentally verified. Fig. 5(a) depicts the spectral evolution of the GS under the P1 oscillation state. By adjusting I_{sl}, the center frequency can be continuously tuned from 12 GHz to 19 GHz. The dependence of the center frequency on I_{sl} is quantified in Fig. 5(b), revealing an approximately linear dependence across the entire tuning range. This linear tuning characteristic indicates that rapid modulation of I_{sl} enables dynamic sweeping of the narrowband GS over a broad frequency range. These features lay the essential foundation for the implementation of Dynamic SAIL.

Subsequently, the feasibility of amplifying wideband frequency-swept signals using the Dynamic SAIL mechanism is experimentally investigated. In the experiment, the triangular LFM waveform generated by an AWG (Keysight 8195A, 65 GSa/s) covers a frequency range of 12 GHz to 16 GHz with a period of 30 μs. To synchronize the GS with the instantaneous frequency of the LFM signal, the injection current of the SL is properly tuned. Due to the inherent nonlinearity of the frequency response in the SL, a pre-compensated control signal is required. As shown in Fig. 6(a), the control signal adopts a dedicated nonlinear profile to ensure the instantaneous GS achieves a linear frequency sweep in the time-frequency domain. Fig. 6(b)

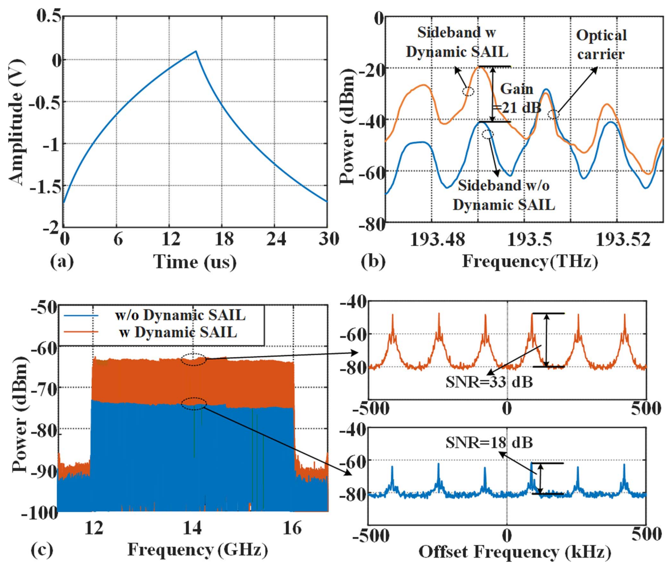

Fig. 6. Experimental results of the Dynamic SAIL mechanism. (a) The pre-compensated control signal waveform applied to the slave laser. (b) Optical spectra of the signal sideband without (blue lines) and with (orange lines) Dynamic SAIL. (c) Electrical spectra of the TFM signal without (blue lines) and with (orange lines) Dynamic SAIL. The insets display the zoomed-in spectral components and the corresponding in-band SNRs.

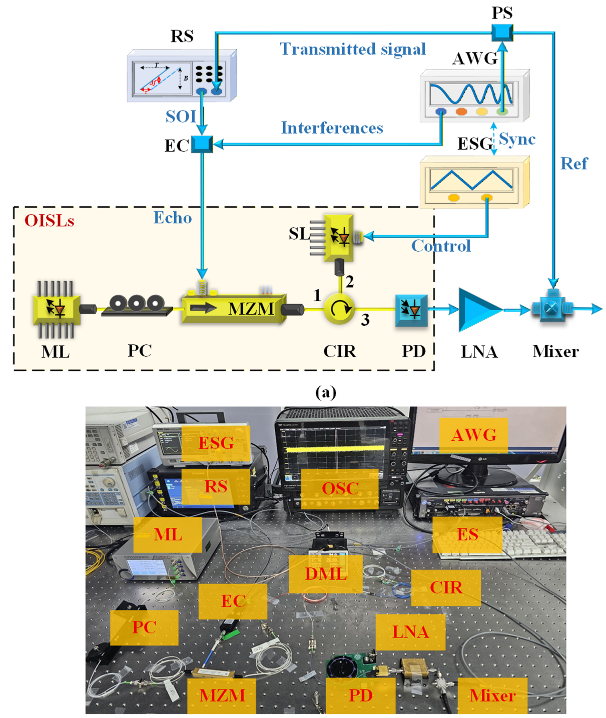

(b)

Fig. 7. The (a) experimental schematic diagram and (b) photograph of the proposed interference-resistant radar reception with the TFM-SSA method.

presents the corresponding optical spectrum. When the Dynamic SAIL is activated, the GS sweeps synchronously with the sweeping optical sideband. Compared to the original sideband (blue lines), the sideband processed by Dynamic SAIL (orange lines) achieves a significant optical power gain of 21 dB. The corresponding electrical spectra of the received LFM signals are compared in Fig. 6(c). The blue line denotes the signal without processing, while the orange line shows the signal processed via the Dynamic SAIL mechanism. It is evident that the system achieves a flat gain across the entire 4 GHz bandwidth. To quantitatively evaluate the signal quality, the fine spectra of individual frequency components are presented in the insets. In the baseline case, the in-band signal-to-noise ratio (SNR) is approximately 18 dB. With Dynamic SAIL implemented, the signal power is effectively enhanced, yielding an improved in-band SNR of 33 dB. The 15 dB enhancement of the in-band SNR verifies that the Dynamic SAIL mechanism can not only boost signal power but also maintain spectral flatness for frequency-swept signals. This provides a solid foundation for interference-resistant radar reception with the Dynamic SAIL-based TFM-SSA method.

B. Interference-Resistant Radar Reception with TFM-SSA

Building on the wideband frequency-swept signal processing capability enabled by Dynamic SAIL mechanism, we further implement interference-resistant radar reception with the TFM-SSA method. The system schematic and photograph are presented in Fig. 7(a) and (b), respectively. The light passes through a polarization controller (PC) and is injected into an MZM (Fujitsu FTM7937EZ) biased at the quadrature point. The modulated optical signal is then directed into an SL (Micro Photons, PL-DFB-1550-C-A81-PA-7-BF) via a CIR. The SL is a commercial 7-pin butterfly-packaged directly modulated distributed feedback (DFB) semiconductor laser. It is biased at 26.8 mA (approximately four times the threshold current) and maintained at a temperature of 26 °C, providing an output optical power of 5.5 dBm. To realize the Dynamic SAIL operation, the SL is directly modulated by a pre-designed control signal generated from a low-speed electrical signal generator (ESG, RIGOL DG4062, 500 MSa/s). For radar signal generation, a triangular LFM waveform is generated by an AWG (Keysight 8195A, 65 GSa/s). This transmitted signal is divided into two branches via an electrical power splitter (PS). One branch serves as the reference signal and is directly fed into the receiving electrical mixer (Marki MM1-0626SSM). The other branch is transmitted to a radar simulator (RS, HQ-RJS-2519P1) to generate the SOI with preset time delays. To simulate the interference environment, the SOI output from the RS is combined with a jamming signal generated by another channel of the AWG through an electrical coupler (EC). The coupled composite signal is then applied to drive the MZM for optical carrier modulation. Notably, the AWG and ESG are strictly synchronized to guarantee precise temporal alignment of all control and radar signals. After optical processing with the TFM-SSA method, the optical signal is sent to a PD for O/E conversion. The processed echo signal is subsequently amplified by an LNA (AT Microwave, LNA-0226-3827, bandwidth: 2–26 GHz, gain: 38 dB) to match the optimal input power range of the electrical mixer. After frequency down-conversion, the de-chirped intermediate-frequency (IF) signal is collected by a real-time oscilloscope (OSC, LeCroy, WaveMaster 8000HD) for further post-processing and analysis.

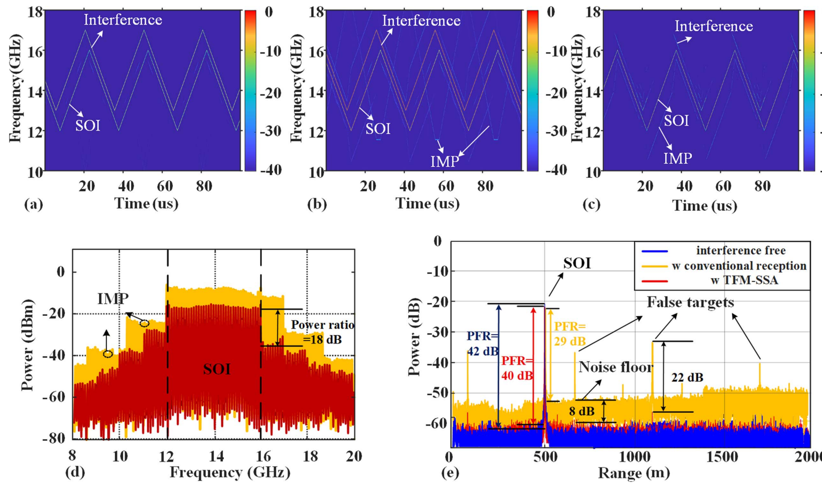

Fig. 8. Experimental results for the parallel interference scenario. The time-frequency diagrams of (a) the original radar echo, (b) the echo amplified by the conventional LNA, and (c) the echo processed by the proposed TFM-SSA. (d) The electrical spectra of the echo after the LNA (yellow lines) and after the TFM-SSA (red lines). (e) The range profiles of the interference-free scenario (blue lines), the echo after the LNA (yellow lines), and the echo after the TFM-SSA (red lines).

In the experiment, the transmitted signal is configured as a triangular LFM signal with a center frequency of 14 GHz, a bandwidth of 4 GHz, and a period of 30 μs. The amplitude (V_{amp}) and offset voltage (V_{offset}) of the control signal are set to 1.85 V and -0.82 V, respectively. The simulated target distance configured in the RS is 500 m. To validate the practical interference-resistant performance of the TFM-SSA method, we first emulate a parallel interference scenario, as depicted in Fig. 8. In this case, the interference adopts a triangular LFM waveform with the same chirp rate as the SOI, while featuring a different center frequency of 15 GHz. The output power of the SOI from the radar simulator and that of the interference signal from the AWG are set as -20 dBm and -6 dBm, respectively. The time-frequency diagram of the original radar echo is presented in Fig. 8(a). Here, the SOI and parallel interference exhibit clear separation in the frequency domain but full overlap in the time domain. For conventional reception schemes, where the echo is directly amplified by the LNA, the in-band strong interference obtains an identical gain. As plotted in Fig. 8(b), this effect drives the LNA into nonlinear saturation, thereby inducing severe spectral regrowth and generating dense IMPs. In contrast, the proposed TFM-SSA method delivers outstanding interference-resistant capability. As shown in Fig. 8(c), driven by the pre-compensated control signal, the instantaneous GS sweeps strictly following the time-frequency characteristics of the SOI. Since the parallel interference maintains a fixed frequency offset relative to the SOI throughout the entire duration, it always falls outside the dynamic amplification window during operation. The corresponding electrical spectrum in Fig. 8(d) provides a quantitative comparison. With conventional reception (yellow lines), the strong interference raises the noise floor and produces abundant IMPs, completely submerging the target SOI. After TFM-SSA processing (red lines), all spurious components are significantly suppressed. Meanwhile, the SOI can be clearly distinguished from the residual interference, achieving a signal-to-interference power ratio improvement of 18 dB. The corresponding range profiles are presented in Fig. 8(e), covering three comparative scenarios: the interference-free condition (blue lines), the scenario with parallel interference (yellow lines), and the result after TFM-SSA processing (red lines). For both the interference-free baseline and the conventional reception schemes, the echo signal is amplified by the LNA and then sent to the electrical mixer directly for de-chirp processing. Under the interference-free condition, the target is detected with a peak-to-floor ratio (PFR) of 42 dB. When parallel interference is introduced (yellow lines), the aforementioned IMPs appear as prominent false targets in the range profile; meanwhile, the overall noise floor rises substantially, and the target PFR degrades to only 29 dB. By applying the proposed TFM-SSA method, these prominent false targets are effectively eliminated, the noise floor is suppressed by approximately 8 dB, and the target PFR is restored to 40 dB. This performance is nearly consistent with that of the interference-free case, representing an obvious 11 dB enhancement in PFR compared with the conventional reception scheme. However, it is worth noting that if the fixed frequency offset of a parallel interference is smaller than the bandwidth of the GS window, it may form a ghost target. Nevertheless, by fine-tuning the time delay of the control signal, the dynamic GS window can be slightly shifted in the time-frequency domain toward the center of the SOI, effectively pushing the adjacent interference out of the passband. Furthermore, from a practical radar system perspective, the actual impact of such ghost targets is highly limited. As indicated in [9], the occurring probability of an in-band ghost target is determined by the ratio of the GS window bandwidth to the total bandwidth of SOI. For our wideband radar system with a sweeping bandwidth of 4 GHz and a GS bandwidth lower bound of approximately 40 MHz, this probability is approximately 1%.

Finally, a cross-interference scenario is conducted to further verify the interference-resistant capability of the TFM-SSA method. The time-frequency diagram of the original echo is illustrated in Fig. 9(a). The interference signal is a conventional up-chirp LFM signal with a chirp rate different from that of the SOI; its center frequency and bandwidth are set to 14

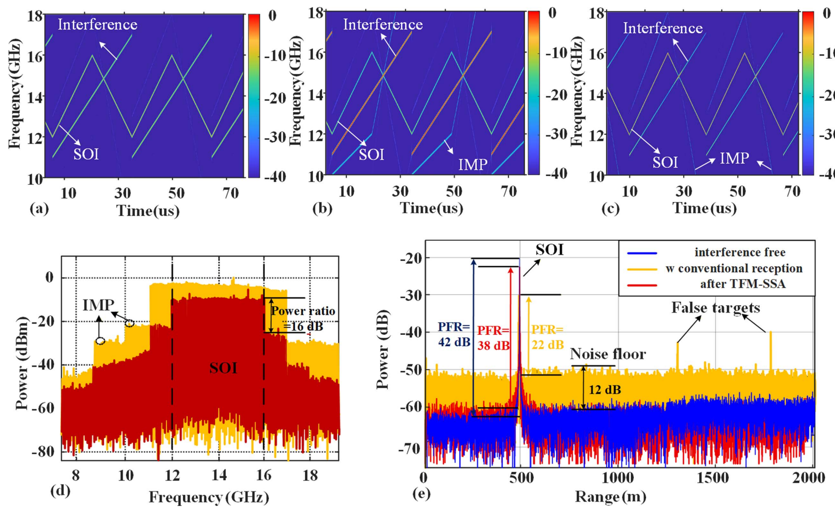

Fig. 9. Experimental results for the cross interference scenario. The time-frequency diagrams of (a) the original radar echo, (b) the echo amplified by the conventional LNA and (c) the echo processed by the proposed TFM-SSA. (d) The electrical spectra of the echo after the LNA (yellow lines) and after the TFM-SSA (red lines). (e) The range profiles of the interference-free scenario (blue lines), the echo after the LNA (yellow lines), and the echo after the TFM-SSA (red lines).

GHz and 6 GHz, respectively. The output powers of SOI and interference signal are set to −20 dBm and −6 dBm, respectively. As shown in Fig. 9(b), similar to the parallel interference scenario, the conventional receiver undergoes severe nonlinear saturation and generates abundant IMPs. Notably, the chirp rates of the SOI (k_{soi}) and interference (k_{int}) are ±0.267 GHz/μs and 0.2 GHz/μs, respectively. Distinct spurious components appear with specific chirp rates of 0.334 GHz/μs ($2k_{\text{soi}}$-k_{int}) and 0.133 GHz/μs ($2k_{\text{int}}$-k_{soi}), indicating that these spurs are third-order IMPs generated by the mixing of the SOI and interference. As depicted in Fig. 9(c), with the TFM-SSA processing, the SOI is effectively amplified while the up-chirp interference and third-order IMPs outside the GS range are significantly suppressed. Although transient amplification occurs at the exact frequency crossing points of the SOI and interference, this frequency overlap is extremely short relative to the 30-μs period, ensuring effective suppression of the total interference energy. The corresponding electrical spectrum in Fig. 9(d) provides a quantitative comparison: compared with the conventional reception scheme (yellow lines), the TFM-SSA method (red lines) markedly suppresses the elevated noise floor and spurious components, achieving a signal-to-interference power ratio improvement of 16 dB. The corresponding range profiles are presented in Fig. 9(e). In the interference-free baseline (blue lines), the target is detected with a PFR of 42 dB. When cross-interference is introduced, the IMPs manifest as an elevated noise floor and false targets in the range profile, leading to a severe degradation of the target PFR to 22 dB. After applying the TFM-SSA method (red lines), these false targets are successfully eliminated, the noise floor is reduced by approximately 12 dB, and the target PFR is recovered to 38 dB. This represents a significant improvement of 16 dB in PFR compared to the conventional reception case. Overall, the TFM-SSA method effectively mitigates the nonlinear saturation of conventional receivers relying on LNAs and BPFs, and prevents the generation of severe IMPs caused by in-band strong interference, thus ensuring reliable target detection in complex interference environments.

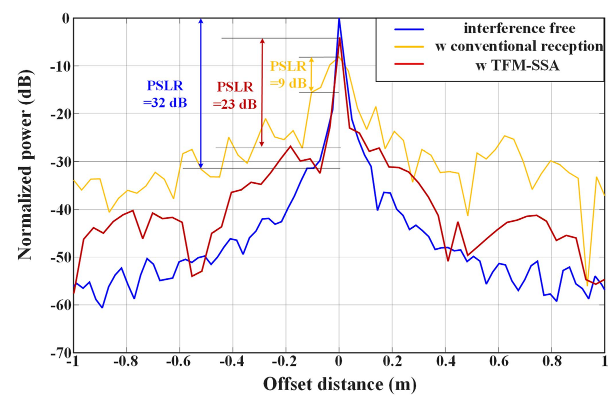

Fig. 10. Range profile comparison of three scenarios: interference-free baseline (blue lines), echo with cross interference after conventional reception (yellow lines), and echo processed by the proposed TFM-SSA (red lines).

To further quantify the impact of the Dynamic SAIL mechanism on the pulse compression performance, the peak-to-sidelobe ratio (PSLR) under the cross interference scenario is examined and presented in Fig. 10. The interference-free baseline yields a PSLR of approximately 32 dB. With TFM-SSA processing, the PSLR reaches approximately 23 dB, exhibiting a degradation of ∼9 dB relative to the interference-free case. This degradation primarily arises from the spontaneous emission noise and relative intensity noise of the slave laser, which are additive and broadband in nature and do not introduce nonlinear phase distortions. In comparison, the conventional receiver under the same strong interference suffers severe LNA saturation, resulting in a drastically degraded PSLR of only ∼9 dB and noticeable mainlobe broadening. It should be clarified that the residual PSLR degradation of the TFM-SSA processed result relative to the interference-free baseline arises not from phase dispersion of the dynamic gain spectrum, but from the additive spontaneous emission noise and relative intensity noise of the SL. Despite this modest degradation, the TFM-SSA method achieves a 14 dB improvement over conventional reception while maintaining a sharp mainlobe, demonstrating its effectiveness in preserving the phase linearity of wideband radar signals under strong in-band interference.

Moreover, the preceding experiments have separately validated the effectiveness of the TFM-SSA method against parallel and cross interference, it is worth noting that this method remains effective when the two types of interference are simultaneously present.

IV. Conclusion

In conclusion, an interference-resistant radar reception method based on TFM-SSA is proposed and experimentally demonstrated to address the severe challenges posed by strong in-band interference. The core foundation of this method lies in the Dynamic SAIL mechanism within an OISL system. By properly controlling the bias current, the instantaneous GS sweeps in strict accordance with the time-frequency characteristics of the SOI. Consequently, the TFM-SSA method selectively amplifies the SOI while effectively suppressing the mismatched interference directly in the optical domain. This prevents the LNA from entering saturation prior to O/E conversion, thereby avoiding the generation of IMPs and spectral regrowth. Comprehensive experiments validate that the proposed system effectively mitigates both parallel and cross interference. The TFM-SSA method suppresses the noise floor by 8 dB and 12 dB, and improves the target PFR by 11 dB and 16 dB in the respective cases, effectively eliminating false targets while enhancing detection sensitivity. Therefore, the proposed method provides a powerful solution for addressing the in-band interference encountered by current radar receivers.

References

[1] H. Zhang et al., "Adaptive FMCW radar interference suppression via coupled range-doppler unsupervised sparse learning and reconstruction," *IEEE Trans. Microw. Theory Techn.*, vol. 73, no. 11, pp. 9442–9458, Nov. 2025.

[2] M. Lei et al., "Demonstration of Photonic Sub-THz ISAC System with Real-Time 251.03-Gbps Communication Rate and Offline 2.5-cm Sensing Resolution," in *Proc. 22nd Int. Conf. Opt. Commun. Netw.*, Harbin, China, 2024, pp. 1–3.

[3] Y. Wang, Q. Zhang, Z. Wei, Y. Lin, and Z. Feng, "Performance analysis of coordinated interference mitigation approach for automotive radar," *IEEE Internet Things J*, vol. 10, no. 13, pp. 11683–11695, Jul. 2023.

[4] G. M. Brooker, "Mutual interference of millimeter-wave radar systems," *IEEE Trans. Electromagn. Compat.*, vol. 49, no. 1, pp. 170–181, Feb. 2007.

[5] S. Alland, W. Stark, M. Ali, and M. Hegde, "Interference in Automotive Radar Systems: Characteristics, Mitigation Techniques, and Current and Future Research," *IEEE Signal Process. Mag.*, vol. 36, no. 5, pp. 45–59, Sep. 2019.

[6] T. Fei, A. Becker, and M. Gardill, "Interference Mitigation in Automotive Radar Systems: A Current State Survey and Future Trends," *IEEE Trans. Intell. Transp. Syst.*, vol. 27, no. 1, pp. 53–80, Jan. 2026.

[7] A. K. Keskin, M. Dagcan Senturk, S. Demirel, A. Kizilay, and A. S. Turk, "Front-end design for Ka band mm-Wave radar," in *Proc. 17th Int. Radar Symp.*, Krakow, Poland, 2016, pp. 1–4.

[8] S. Lee, J.-Y. Lee, and S.-C. Kim, "Mutual Interference Suppression Using Wavelet Denoising in Automotive FMCW Radar Systems," *IEEE Trans. Microw. Theory Techn.*, vol. 22, no. 2, pp. 887–897, Feb. 2021.

[9] F. Jin and S. Cao, "Automotive radar interference mitigation using adaptive noise canceller," *IEEE Trans. Veh. Technol.*, vol. 68, no. 4, pp. 3747–3754, Apr. 2019.

[10] Y. Li, C. Wang, F. Li, X. Han, and Y. Song, "An adaptive interference cancellation method for automotive FMCW radar based on waveform optimization," in *Proc. IET Int. Radar Conf., Online Conf.*, 2020, pp. 666–670.

[11] J. Wang, "CFAR-based interference mitigation for FMCW automotive radar systems," *IEEE Trans. Intell. Transp. Syst.*, vol. 23, no. 8, pp. 12229–12238, Aug. 2022.

[12] J. Roessler et al., "Design of a Decade-Bandwidth Tunable Multi-Notch Filter for RFI Mitigation in a Congested Spectral Environment," in *Proc. United States Nat. Committee URSI Nat. Radio Sci. Meeting*, Boulder, CO, USA, 2025, p. 4.

[13] J. Yao, "Microwave photonics," *J. Lightw. Technol.*, vol. 27, no. 3, pp. 314–335, Feb. 2009.

[14] X. Zhang et al., "Weak RF signals detection based on all-optical multimode oscillation with high performance," *Opt. Exp.*, vol. 34, no. 3, pp. 4307–4317, Feb. 2026.

[15] X. Yu et al., "Broadband Frequency-hopping Radar with Fourier Domain Mode-locking Period-one Laser Dynamics," *IEEE Photon. Technol. Lett.*, vol. 37, no. 19, pp. 1105–1108, Oct. 2025.

[16] H. Wang, A. Wen, Y. Men, and Y. Wang., "Photonics-based radar jamming signal generation and self-interference cancellation," *J. Lightw. Technol.*, vol. 41, no. 18, pp. 5922–5929, Sep. 2023.

[17] S. Wang et al., "Optical adaptive multi-path wideband self-interference cancellation system based on the particle swarm optimization," in *Proc. 7th Glob. Intell. Ind. Conf.*, SPIE, Bellingham, WA, 2024, pp. 405–408.

[18] Y. Xing, S. Li, X. Chen, X. Xue, and X. Zheng, "Optical multi-tap RF canceller for in-band full-duplex wireless communication systems," *IEEE Photon. J.*, vol. 14, no. 5, Oct. 2022, Art. no. 5554407.

[19] X. Han, B. Huo, Y. Shao, C. Wang, and M. Zhao, "RF self-interference cancellation using phase modulation and optical sideband filtering," *IEEE Photon. Technol. Lett.*, vol. 29, no. 11, pp. 917–920, Jun. 2017.

[20] L. Xing, S. Li, X. Xue, X. Zheng, and B. Zhou, "Multiband Radar Using Microwave Photonic Time-Frequency Limiter for Real-Time Detection in Interference Scenarios," *IEEE Photon. J.*, vol. 17, no. 2, Apr. 2025, Art. no. 5500108.

[21] X. Yu et al., "Broadband stepped-frequency radar waveform generation by Fourier domain mode-locking period-one laser dynamics," *Opt. Lett.*, vol. 49, pp. 4266–4269, 2024.

[22] X. Yu et al., "Microwave generation by P2 dynamics of optically injected semiconductor laser," *J. Lightw. Technol.*, vol. 43, no. 10, pp. 4895–4902, May 2025.

[23] G. Sun et al., "Photonics-based MIMO radar with broadband digital coincidence imaging," *Trans. Microw. Theory Techn.*, vol. 72, no. 12, pp. 6996–7003, Dec. 2024.

[24] P. Zhou, F. Zhang, D. Zhang, and S. Pan, "Performance enhancement of an optically injected semiconductor laser based optoelectronic oscillator by subharmonic microwave modulation," *Opt. Lett.*, vol. 43, no. 21, pp. 5439 5442, 2018.

[25] H. Chen, M. Lee, Y. H. Won, B. Nakarmi, and S. Pan, "High-speed switchable dual-passband microwave photonic filter with dual-beam injection in an SMFP-LD," *J. Lightw. Technol.*, vol. 39, no. 24, pp. 7966–7972, Dec. 2021.

[26] K. Dergachov, E. Ovdiyuk, and V. Dubinin, "Comparative Analysis Region of Interest (ROI) Tracking Methods," in *ICTM Lecture Notes in Networks and Systems*. Cham, Switzerland: Springer, 2024.

[27] M. Mesmakhosroshahi, J. Kim, Y. Lee, and J.-b. Kim, "Stereo based region of interest generation for pedestrian detection in driver assistance systems," in *Proc. IEEE Int. Conf. Image Process.*, Melbourne, VIC, Australia, 2013, pp. 3386–3389.

[28] X. Zhang et al., "Integrated Direct Single Sideband Modulation Utilizing Sideband Amplification Injection Locking Effect Based on Multi-Section Mutual Injection DFB Laser," *J. Lightw. Technol.*, vol. 39, no. 6, pp. 1645–1652, Mar. 2021.

[29] S. L. Woodward et al., "A DBR laser tunable by resistive heating," *IEEE Photon. Technol. Lett.*, vol. 4, no. 12, pp. 1330–1332, Dec. 1992.

[30] H. Zhang et al., "Optical parametric-assist frequency modulation for FMCW Lidar enabling double-range velocity measurement," *Opt. Lasers Eng.*, vol. 178, 2024, Art. no. 108203.

[31] Y. Lu et al., "Highly Efficient Algorithm for Frequency Linearization in FMCW Lidar Using Directly-Modulated DFB Laser," in *Proc. Opt. Fiber Commun. Conf.*, San Francisco, CA, USA, 2025, pp. 1–3.

[32] M. AlMulla and J.-M. Liu, "Effects of the linewidth enhancement factor on the microwave linewidth of the period-one oscillations of optically injected semiconductor lasers," *Opt. Lett.*, vol. 47, pp. 1166–1169, 2022.

[33] L. Goldberg, H. Taylor, and J. Weller, "FM sideband injection locking of diode lasers," *Electron. Lett.*, vol. 18, pp. 1019–1020, 1982.